Synthetic Metals 161 (2011) 489–495

Contents lists available at ScienceDirect

Synthetic Metals

journal homepage: www.elsevier.com/locate/synmet

Tuning the electronic properties of monolayer graphene by the periodic aligned graphene nanoribbons

C.H. Lee[a], S.C. Chen[b], W.S. Su[c], R.B. Chen[d,*], M.F. Lin[b,**]

[a] Institute of Applied Physics, National Chengchi University, Taipei City 116, Taiwan
[b] Department of Physics, National Cheng Kung University, Tainan 701, Taiwan
[c] Center for General Education, Tainan University of Technology, Tainan 710, Taiwan
[d] Center of General Education, National Kaohsiung Marine University, Kaohsiung 811, Taiwan

ARTICLE INFO

Article history:
Received 19 September 2010
Received in revised form
28 November 2010
Accepted 2 January 2011
Available online 5 February 2011

PACS:
71.20.Tx, 73.20.−r, 73.21.−b

Keywords:
Graphene nanoribbons
Monolayer graphene
Electronic properties

ABSTRACT

The $2p_z$ tight-binding model has been used to investigate the electronic properties of ribbon–graphene hybrid systems. This system is constructed by zigzag graphene nanoribbons aligned periodically on monolayer graphene. It was found that for such systems the electronic properties would be strongly influenced by the geometric structure of graphene nanoribbons, such as the width and the period of the ribbons. In addition, the stacking arrangement between graphene nanoribbons and monolayer graphene also plays a dominant role in determining the band structures in the low-energy region. These geometric structure effects can be well understood through the density of state calculations. Such hybrid structures lead to interesting novel features, dissimilar from those of single layer graphene, and could serve as a platform for the studies of device applications.

1. Introduction

Graphite is a carbon-related material with three-dimensionality. The most common form of graphite, known as Bernal graphite, is of hexagonal symmetry and is layered in ABAB-manner stacking. For these graphitic-based structures, many studies have been reported in both experimental [1–3] and theoretical [4–7] aspects. As for the few-layer graphenes, they are candidates for the studies of two-dimensional (2D) physical phenomena. Theoretical investigations into the electronic properties of such a system have been made using the tight-binding model [8,9] and density functional theory [10,11]. It is found that the energy dispersion near the Fermi level (E_F) is sensitive to the stacking arrangement as well as the layer number. Recently, the few-layer graphenes are discovered through mechanical friction [12,13] and thermal decomposition [14,15]. Moreover, monolayer and bilayer graphenes also display unconventional quantum Hall effects in transport properties [16,17].

A quasi-one-dimensional (Q1D) graphene nanoribbon can be constructed by cutting the monolayer graphene along a specific direction, and it is essentially a trim of graphene with a finite width in nanometer size. The zigzag and armchair graphene nanoribbons, which have been usually investigated, are a graphene nanoribbon with zigzag and armchair shaped edges, respectively. Such fascinating materials could be produced by many physical treatments and chemical synthesis [18–21], and have gained much attention due to their novel electronic structures. For a zigzag ribbon, its band structures own the partial flat bands due to the contributions of the carbon atoms on the ribbon edge, while for an armchair ribbon, the electronic properties depend on its width. Besides, their magnetic and optical properties have also been studied and reported theoretically [22–25].

The hybrid systems of the carbon-related material could present a platform to study the influences of the interface states. Very recently, the carbon nanotube–graphene hybrids have been made to fabricate [26]. Q1D carbon nanotubes are distributed on the 2D graphene. It would be desirable to replace carbon nanotubes by graphene nanoribbons because of the unique edger structures in graphene nanoribbons. In this work, we investigated the electronic properties of zigzag ribbon–graphene hybrid systems through the $2p_z$ tight-binding model. The interlayer interactions are taken into account, and the effects for ribbon with various widths and periods are also studied and presented.

* Corresponding author. Tel.: +886 73617141x3671; fax: +886 73648120.
** Corresponding author. Tel.: +886 6 2757575x65272; fax: +886 6 2747995.
E-mail addresses: rbchen@mail.nkmu.edu.tw (R.B. Chen), mflin@mail.ncku.edu.tw (M.F. Lin).

0379-6779/$ – see front matter © 2011 Elsevier B.V. All rights reserved.
doi:10.1016/j.synthmet.2011.01.003

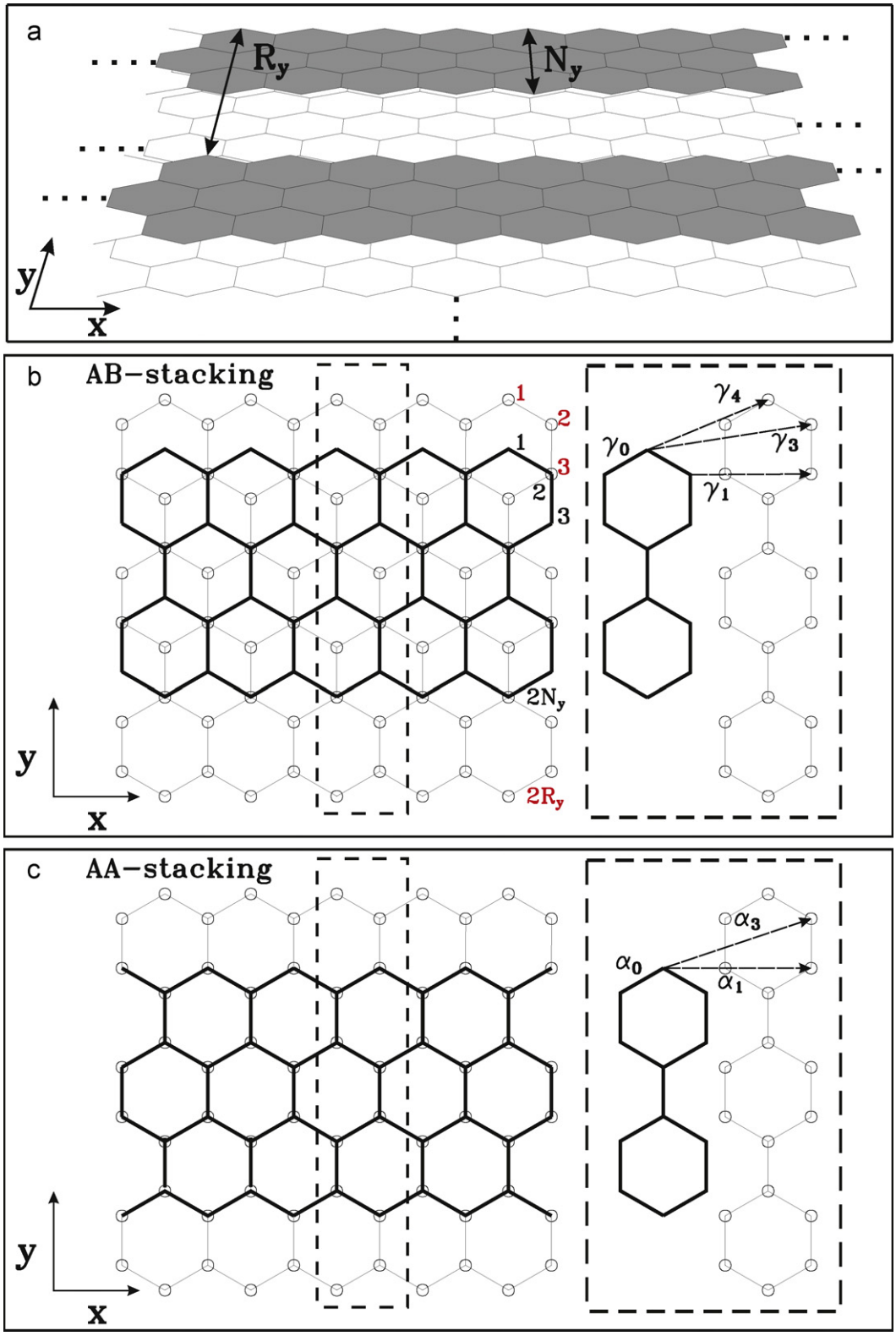

Fig. 1. (a) The geometric structure of zigzag ribbon–graphene hybrid system. N_y and R_y represent the ribbon width and period, respectively. (b) The ribbon is projected onto the graphene with the thick black lines in the AB-stacked hybrid system. γ_0 is the intralayer interaction and γ_i's indicate the interlayer interactions. (c) Same plot as (b), but shown for the AA-stacked hybrid system.

2. Theory

The geometric structure of zigzag ribbon–graphene hybrid system is sketched in Fig. 1(a). The ribbons with a width N_y are aligned on the graphene with a period R_y along the y-axis, where N_y and R_y denote the numbers of the zigzag lines. The carbon atom on the edge of zigzag ribbon is terminated by a hydrogen atom, and it is stable at extremely low hydrogen concentrations. The sp^2-bonding configuration on the graphene layer keeps unchanged. The C–C bond length is $b = 1.42$ Å, and the interlayer distance between ribbon and

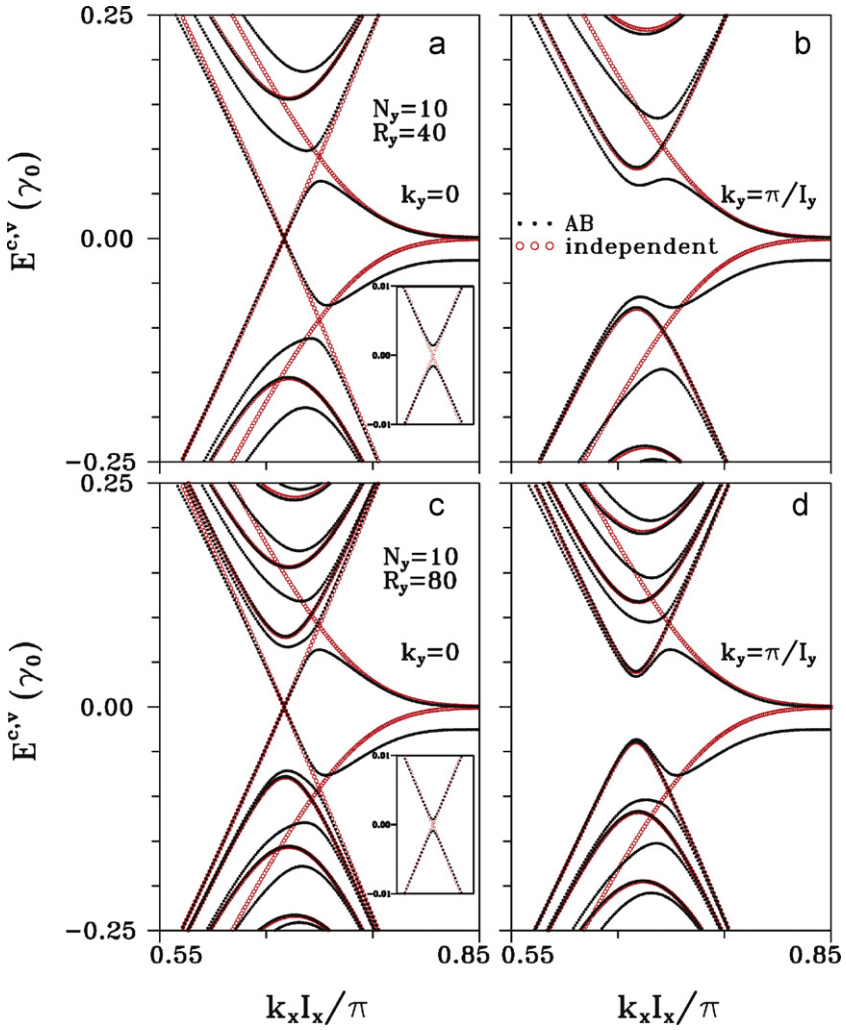

Fig. 2. The energy dispersion of the zigzag ribbon–graphene system ($N_y = 10$, $R_y = 40$) at (a) $k_y = 0$ and (b) $k_y = \pi/I_y$. The independent and AB-stacked systems are represented by open and solid circles, respectively. (c) and (d) are the same plots as (a) and (b), but with ($N_y = 10$, $R_y = 80$). The insets in (a) and (c) show the energy gap near E_F.

graphene is assumed to be 3.35 Å, which is the same as that of the graphite. The unit cell of such a system has $(2N_y + 2R_y)$ carbon atoms, where its periodical lengths along the x-axis and y-axis are $I_x = \sqrt{3}b$ and $I_y = (3b/2)R_y$, respectively. The first Brillouin zone is defined by $-\pi/I_x \le k_x \le \pi/I_x$ and $-\pi/I_y \le k_y \le \pi/I_y$.

Under the tight-binding model with the $2p_z$-orbitals of the carbon atoms, the Hamiltonian matrix could be represented as

$$H = \begin{pmatrix} h_1 & h_{12} \\ h_{12}^* & h_2 \end{pmatrix}.$$

The block h_1 is a $2N_y \times 2N_y$ Hamiltonian matrix of the zigzag graphene nanoribbon, whereas h_2 is a $2R_y \times 2R_y$ Hamiltonian matrix of the monolayer graphene. The elements of the h_1 and h_2 are given by

$$(h_{ij})_1 = \begin{cases} \gamma_6 & \text{if } j = i, \quad i \text{ is even;} \\ 2\gamma_0 e^{-ik_y b/2}\cos(\sqrt{3}bk_x/2) & \text{if } j = i+1, \quad i \text{ is odd;} \\ \gamma_0 e^{-ik_y b} & \text{if } j = i+1, \quad i \text{ is even;} \\ 0 & \text{others.} \end{cases} \tag{1}$$

and

$$(h_{ij})_2 = \begin{cases} \gamma_6 & \text{if } j = i, \quad i \text{ is odd}, \quad i < 2N_y + 2; \\ 2\gamma_0 e^{-ik_y b/2}\cos(\sqrt{3}bk_x/2) & \text{if } j = i+1, \quad i \text{ is odd;} \\ \gamma_0 e^{-ik_y b} & \text{if } j = i+1, \quad i \text{ is even;} \\ \gamma_0 e^{ik_y b} & \text{if } i = 1, \quad j = 2R_y; \\ 0 & \text{others.} \end{cases} \tag{2}$$

respectively. In this study, the zigzag graphene nanoribbon and monolayer graphene are arranged according to Bernal (AB) stacking, as shown in Fig. 1(b). There exists a different value γ_6 between the on-site energy of A atom and that of B atom due to such a AB manner. In the ribbon (graphene), the A atom corresponds to the ith atom, in which i equals even integer (odd integer).

Furthermore, h_{12} describes the interactions of the $2p_z$ orbitals between the graphene nanoribbon and monolayer graphene with AB-stacking. They can be expressed as

$$(h_{ij})_{12} = \begin{cases} \gamma_4 e^{ik_y b} & \text{if } j = i, \quad i \text{ is odd;} \\ \gamma_3 e^{ik_y b/2}\cos(\sqrt{3}bk_x/2) & \text{if } j = i+1, \quad i \text{ is odd;} \\ \gamma_4 e^{-ik_y b/2}\cos(\sqrt{3}bk_x/2) & \text{if } j = i+2, \quad i \text{ is odd;} \\ \gamma_3 e^{-ik_y b} & \text{if } j = i+3, \quad i \text{ is odd;} \\ \gamma_4 e^{ik_y b} & \text{if } j = i, \quad i \text{ is even;} \\ \gamma_1 & \text{if } j = i+1, \quad i \text{ is even;} \\ \gamma_4 e^{-ik_y b/2}\cos(\sqrt{3}bk_x/2) & \text{if } j = i+2, \quad i \text{ is even;} \\ 0 & \text{others.} \end{cases} \tag{3}$$

γ_0 and γ_i's indicate the intralayer interactions and the interlayer interactions, respectively, which correspond to the values of the AB-stacked graphite [5,6]. They are $\gamma_0 = 2.598$ eV, $\gamma_1 = 0.364$ eV, $\gamma_3 = 0.319$ eV, $\gamma_4 = 0.177$ eV, and $\gamma_6 = -0.026$ eV.

Another arrangement in this hybrid system is the simple hexagonal (AA) stacking, as plotted in Fig. 1(c). In such a AA-stacking, all carbon atoms of the ribbon are projected directly onto those of the

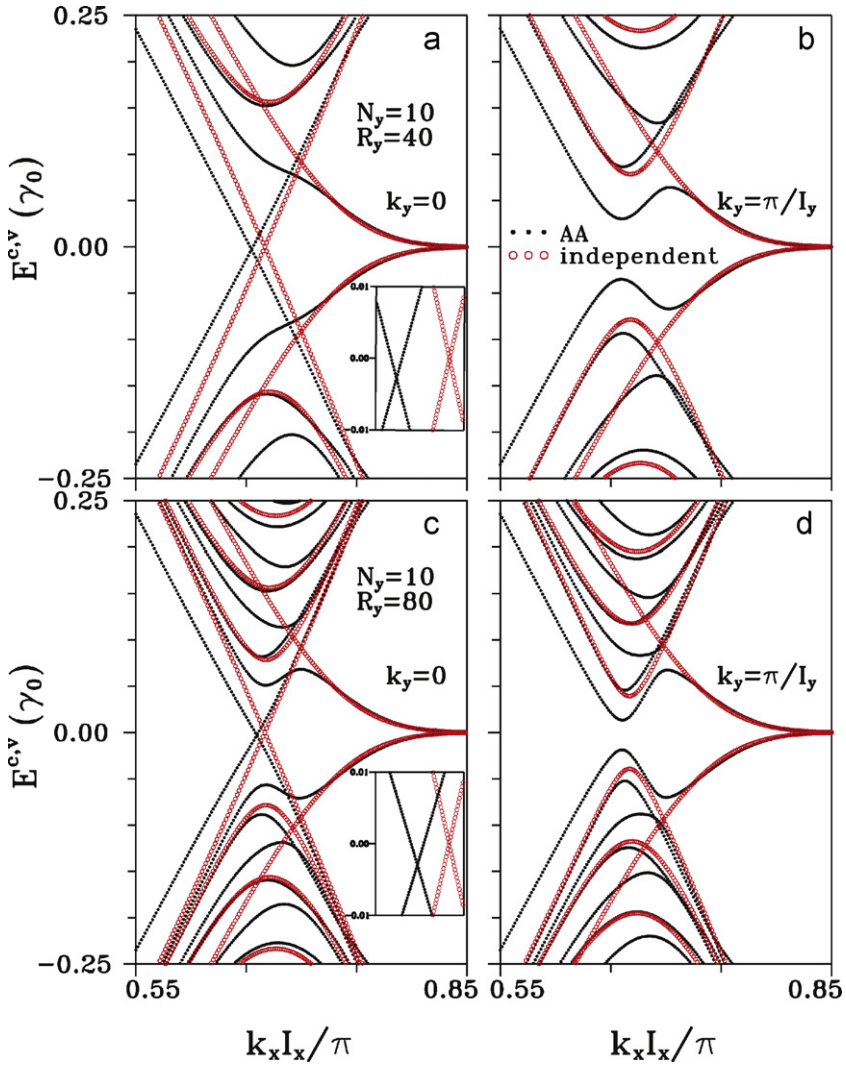

Fig. 3. Same plot as Fig. 2, but shown for the AA-stacking.

graphene. The corresponding intralayer and interlayer Hamiltonian elements can be expressed as follows:

$$(h_{ij})_1 = \begin{cases} 2\alpha_0 e^{-ik_y b/2}\cos(\sqrt{3}bk_x/2) & \text{if } j=i+1, \quad i \text{ is odd;} \\ \alpha_0 e^{-ik_y b} & \text{if } j=i+1, \quad i \text{ is even;} \\ 0 & \text{others,} \end{cases} \tag{4}$$

$$(h_{ij})_2 = \begin{cases} 2\alpha_0 e^{-ik_y b/2}\cos(\sqrt{3}bk_x/2) & \text{if } j=i+1, \quad i \text{ is odd;} \\ \alpha_0 e^{-ik_y b} & \text{if } j=i+1, \quad i \text{ is even;} \\ \alpha_0 e^{ik_y b} & \text{if } i=1, \quad j=2R_y; \\ 0 & \text{others,} \end{cases} \tag{5}$$

and

$$(h_{ij})_{12} = \begin{cases} \alpha_1 & \text{if } j=i+2, \\ \alpha_3 e^{ik_y b} & \text{if } j=i+1, \quad i \text{ is odd;} \\ \alpha_3 e^{-ik_y b/2}\cos(\sqrt{3}bk_x/2) & \text{if } j=i+3, \quad i \text{ is odd;} \\ \alpha_3 e^{ik_y b/2}\cos(\sqrt{3}bk_x/2) & \text{if } j=i+1, \quad i \text{ is even;} \\ \alpha_3 e^{-ik_y b} & \text{if } j=i+3, \quad i \text{ is even;} \\ 0 & \text{others.} \end{cases} \tag{6}$$

The hopping integrals α_0, α_1, and α_3 are taken from the simple hexagonal graphite in Ref. [5]. Through diagonalizing the Hamiltonian matrix, energy dispersion $E^{c,v}$ can be obtained, where the superscripts c and v represent the conduction π^* band and valence π band, respectively.

3. Results and discussion

Fig. 2(a) shows the band structures of the zigzag ribbon––graphene hybrid system ($N_y = 10$, $R_y = 40$) at $k_y = 0$. We only consider the band structure against k_x with I_y greater than I_x. For the independent system (open circle), the low-energy band structures consist of the linear bands and partial flat bands. The linear bands, which intersect at $E_F = 0$ and $k_x = 2\pi/3I_x$, belong to the monolayer graphene, while the zigzag ribbon owns partial flat bands, which are dispersionless over $k_x \sim 0.85\pi/I_x$. In the zigzag ribbon case, their eigenfunctions for such partial flat bands are located on the outmost carbon atoms of the ribbon. With the consideration of the interlayer interactions of AB-stacking (solid circles), the band structures are drastically changed. Obviously, the liner bands change into the parabolic bands with an energy gap ($\sim 3 \times 10^{-3}\gamma_0$) emerging at $k_x = 2\pi/3I_x$, as shown in the inset of Fig. 2(a). In addition, their wavefunctions are also modified by the interlayer interactions. For the parabolic band at $k_x = 2\pi/3I_x$ above the $E_F = 0$, the contributions for eigenfunctions still come from the graphene, mainly the B atoms, whereas the B atoms of ribbon and A atoms of graphene dominate the band below the $E_F = 0$ (the inset of Fig. 2(a)). As k_x shifts slightly away from $2\pi/3I_x$, the band structures are gradually influenced by the ribbon. For instance, at $k_x \sim 0.7\pi/I_x$, the intersection of the two bands from graphene and ribbon above the E_F is broken because of the interlayer interactions. It is found

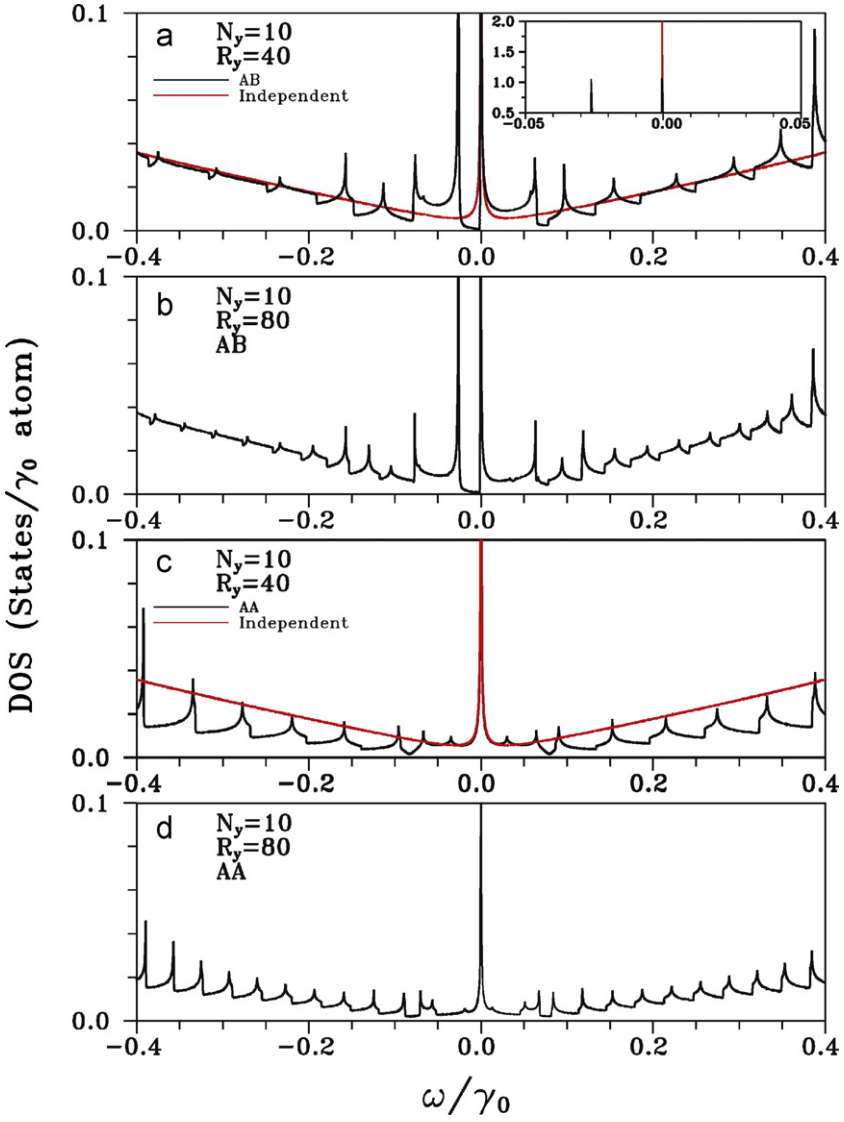

Fig. 4. Density of states (DOS) is calculated for $N_y = 10$ zigzag ribbons with AB-stacking for the period (a) $R_y = 40$ and (b) $R_y = 80$. (c) and (d) are the same plots as (a) and (b), but with AA-stacking. The independent system is also shown.

that the lower band is contributed mostly by the ribbon, especially the edge carbon atoms, while the contributions for the higher band come from the ribbon and from the atoms of graphene which are away from the overlap of ribbon and graphene. Moreover, the partial flat band will also be separated. This is because that the B atoms at the edge of the ribbon are projected to the center of hexagon in the graphene, whereas the A atoms are projected on the A atom of graphene, as presented in Fig. 1(b).

Fig. 2(b) shows the system with different band structures at $k_y = \pi/I_y$. Without interlayer interactions, one can see that the partial flat bands from the ribbon do not disappear. For the low energy region, doubly degenerate parabolic bands appear, which are contributed from the graphene. With the consideration of the interlayer interactions, the degenerate parabolic bands are separated and new band-edge states occur. As k_x increases, the contributions of the parabolic band nearest E_F from the ribbon would gradually rise, while those from graphene decrease. In contrast, the other parabolic band is hardly affected and its contributions are mostly from the graphene.

Now, consider the effect of the period of ribbons on the graphene in this hybrid system. The energy dispersions with double period $R_y = 80$ are calculated along the k_x at $k_y = 0$ as well as $k_y = \pi/I_y$, as shown in Fig. 2(c) and (d), respectively. Since the period becomes larger, band structures are folded into smaller first Brillouin zone, which results in more degenerate states at $k_y = 0$ and $k_y = \pi/I_y$. Such degeneracies are further destroyed by the interlayer interactions so that many band-edge states appear at larger R_y. Moreover, the energy gap is also affected by the period of the ribbon. For example, in the inset of Fig. 2(c), E_g ($\sim 1.6 \times 10^{-3}\gamma_0$) is smaller than that with $R_y = 40$. Meanwhile, the energy spacing between the valence and conduction parabolic bands at $k_y = \pi/I_y$ decreases as the R_y increases, as illustrated in Fig. 2(d).

In Fig. 3(a), the low-energy band structures of the AA-stacked hybrid system are different from those of the AB-stacked one. It is found that not only the partial flat bands could not be separated but also the intersection of the linear bands could not be destroyed by the interlayer interactions. However, the partial flat bands would be shifted upwards a little bit and cause a slight shift of the E_F from the intersection of the linear bands, as shown in the inset of Fig. 3(a), where the intersection of the linear bands does not locate at $2\pi/3I_x$. On the other hand, the tight-binding functions of the linear bands mainly come from the overlapping carbon atoms of the ribbon and graphene. In Fig. 3(b), the degeneracy of parabolic bands is also destroyed. The parabolic band, which is hardly affected by

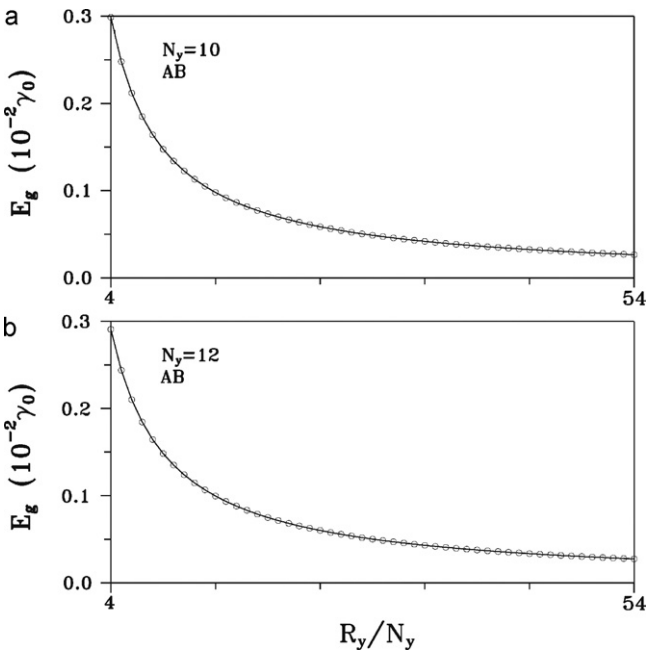

Fig. 5. The R_y-dependent energy gaps of the hybrid system with (a) $N_y = 10$ and (b) $N_y = 12$.

the interlayer interactions with AB-stacking, would be changed and their contribution from ribbon would increase with k_x rising. With the period doubles, the wavevector of the intersection of the linear bands would get closer to $2\pi/3I_x$, and more band edges occur at $k_y = 0$ and $k_y = \pi/I_y$, as shown in Fig. 3(c) and (d).

From the density of states (DOS) point of view, the properties of the band structures for such a hybrid system can be well understood. The definition of DOS is given by

$$D(\omega) = \frac{2I_xI_y}{2(N_y + R_y)} \sum_{h=c,v} \int_{1stBZ} \frac{dk_x dk_y}{4\pi^3} \frac{\Gamma}{[(E^h(k_x, k_y) - \omega)^2 + \Gamma^2]} \quad (7)$$

Γ ($= 10^{-4}\gamma_0$) is the phenomenological broadening parameter. In the independent system, the DOS is symmetrical at $\omega = 0$ (Fig. 4(a)). There exists a delta-function-like peak, which originates from the partial flat bands in the ribbon. However, the strength of DOS has a linear dependence on the frequency except around $\omega = 0$, which results from the single-layer graphene. When the interlayer interactions are taken into account for AA- and AB-stacking, the DOS ($N_y = 10$, $R_y = 40$) would be drastically changed, and the symmetry of the peaks at $\omega = 0$ could be broken. The delta-function-like peak would be split into two lower peaks in the inset of Fig. 4(a), and an energy gap would occur between the two peaks. As a result, many quasi-1D peaks appear due to the parabolic subbands, and their peak frequencies correspond to the state energies of the band-edge states. More peaks would appear because of the expansion of the ribbon period and the occurrence of more band-edge states in the energy dispersions, as shown in Fig. 4(b). These small peaks near the E_F could provide more new excitation channels and are expected to affect the low-energy optical absorption peaks. In Fig. 4(c), the delta-function-like peak at $E_F = 0$ could not be altered. Besides, the peaks at $0.2\gamma_0 \le |\omega| \le 0.4\gamma_0$ are very similar to 1D behavior in comparison with AB-stacking, and it could be concluded that the AA-stacked energy dispersions along k_y are weaker than the AB-stacked ones. When R_y increases, more Q1D peaks appear at low energy, which is similar to the case of Fig. 4(b), as presented in Fig. 4(d).

Fig. 5(a) and (b) shows the energy gap of the AB-stacked hybrid system against R_y/N_y with $N_y = 10$ and $N_y = 12$, respectively. In Fig. 5(a), E_g has strong dependence on ribbon period R_y. As R_y increases, E_g decreases sharply at first and then gradually slow down the descending speed. For such a case, the energy gap occurs at $k_x = 2\pi/3I_x$ and $k_y = 0$, which is the same location as that of the linear bands intersecting without the interlayer interactions. Moreover, the expansion of the ribbon period would lead to different influences on the two parabolic bands near $E_F = 0$. The band above E_F is not relevant to the ribbon, but the band below E_F can be affected by R_y and N_y. As $N_y = 12$, a similar tendency toward Fig. 5(a) can be observed, as shown in Fig. 5(b). As a result, the energy gap could be effectively modulated by the width and period of the ribbon.

4. Conclusions

Our results show that such a hybrid system is closely related to the edge structure, the width and the period of ribbon, as well as the stacking types. Although the zigzag ribbon possesses the partial flat bands at low energy, the AB-stacking could separate the partial flat bands from the ribbon, break the intersection of the linear bands from the graphene, and induce an energy gap. Moreover, E_g could be modified by varying N_y and R_y. In contrast, the AA-stacking would only slightly shift the partial flat bands, make the Fermi level leaving the intersection of the linear bands, and thus the free carriers could exist at E_F. The enlargement of the ribbon period induces the folding of the first Brillouin zone, which makes more band-edge states appear in the reduced first Brillouin zone. The above-mentioned changes in the band structures could also be observed in DOS, for example, the split of delta-function-like peak and the occurrence of more peaks. The stacking type of the hybrid system would modify the optical and transport properties. Our findings would open up more possibilities in designing nanoelectronic and nanomechanical devices.

Besides, in the pure zigzag graphene nanoribbon without hydrogen, the carbon atoms near the edge would undergo rearrangement and their C–C bonds have the z-axis component. In other words, there exist the sp^2-bonding and sp^3-bonding configurations simultaneously. The effect of rearrangement on electronic properties is worth investigating further. On the other hand, the spin-wavefunction calculations will be predicted to influence the low-energy band structures. The similar changes can be observed from the previous study on the graphene nanotube–nanoribbon system [27]. When the width of the ribbon increases, the effect of the spin–spin interaction gradually reduces.

Acknowledgments

This work was supported by the NSC and NCTS of Taiwan, under the grant nos. NSC 95-2112-M-022-001-MY2 and NSC 95-2112-M-006-028-MY3.

References

[1] M.S. Dresselhaus, G. Dresselhaus, Adv. Phys. 30 (1981) 139.
[2] D.E. Soule, Phys. Rev. 112 (1958) 698.
[3] G. Li, E.Y. Andrei, Nat. Phys. 3 (2007) 623.
[4] P.R. Wallace, Phys. Rev. 71 (1947) 622.
[5] J.C. Charlier, J.-P. Michenaud, X. Gonze, Phys. Rev. B 46 (1992) 4531.
[6] J.C. Charlier, J.-P. Michenaud, X. Gonze, J.-P. Vigneron, Phys. Rev. B 44 (1991) 13237.
[7] F.L. Shyu, M.F. Lin, J. Phys. Soc. Jpn. 69 (2000) 3781.
[8] B. Partoens, F.M. Peeters, Phys. Rev. B 74 (2006) 075404.
[9] E. McCann, Phys. Rev. B 74 (2006) 161403(R).
[10] S. Latil, L. Henrard, Phys. Rev. Lett. 97 (2007) 036803.
[11] J.H. Ho, Y.H. Chiu, S.J. Tsai, M.F. Lin, Phys. Rev. B 79 (2009) 115427.
[12] K.S. Novoselov, A.K. Geim, S.V. Morozov, D. Jiang, Y. Zhang, S.V. Dubonos, I.V. Grigorieva, A.A. Firsov, Science 306 (2004) 666.
[13] K.S. Novoselov, A.K. Geim, S.V. Morozov, D. Jiang, M.I. Katsnelson, I.V. Grigorieva, S.V. Dubonos, A.A. Firsov, Nature (London) 438 (2005) 197.

[14] C. Berger, Z.M. Song, T.B. Li, X.B. Li, A.Y. Ogbazghi, R. Feng, Z.T. Dai, A.N. Marchenkov, E.H. Conrad, P.N. First, W.A. de Heer, J. Phys. Chem. B 108 (2004) 19912.
[15] C. Berger, Z. Song, X. Li, X. Wu, N. Brown, C. Naud, D. Mayou, T. Li, J. Hass, A.N. Marchenkov, E.H. Conrad, P.N. First, W.A. de Heer, Science 312 (2006) 1191.
[16] Y. Zhang, Y.W. Tan, H.L. Stormer, P. Kim, Nature (London) 438 (2005) 201.
[17] K.S. Novoselov, E. McCann, S.V. Morozov, V.I. Fal'ko, M.I. Katsnelson, U. Zeitler, D. Jiang, F. Schedin, A.K. Geim, Nat. Phys. 2 (2006) 177.
[18] M. Murakami, S. Iijima, S. Yoshimura, J. Appl. Phys. 60 (1986) 3856.
[19] B.L.V. Prasad, H. Sato, T. Enoki, Y. Hishiyama, Y. Kaburagi, A.M. Rao, P.C. Eklund, K. Oshida, M. Endo, Phys. Rev. B 62 (2000) 11209.
[20] M. Yudasaka, Y. Tasaka, M. Tanaka, H. Kamo, Y. Ohki, S. Usami, Appl. Phys. Lett. 64 (1994) 3237.
[21] M. Zhang, D.H. Wu, C.L. Xu, Y.F. Xu, W.K. Wang, Nanostruct. Mater. 10 (1998) 1145.
[22] K. Nakada, M. Fujita, G. Dresselhaus, M.S. Dresselhaus, et al., Phys. Rev. B 54 (1996) 17954.
[23] K. Harigaya, Chem. Phys. Lett. 340 (2001) 123.
[24] K. Kusakabe, M. Maruyama, Phys. Rev. B 67 (2003) 092406.
[25] F.L. Shyu, M.F. Lin, J. Phys. Soc. Jpn. 69 (2000) 3529.
[26] D. Yu, L. Dai, J. Phys. Chem. Lett. 1 (2010) 467.
[27] C.H. Lee, C.K. Yang, M.F. Lin, C.P. Chang, W.S. Su, Phys. Chem. Chem. Phys. (2011), doi:10.1039/C0CP01569E.